DOI 10.1007/s11062-019-09780-1
Neurophysiology, Vol. 50, No. 6, November, 2018

DISCUSSIONS

Three-Dimensional Representation of Equilibrium Joint Torques in Two-Joint Movements of the Upper Limb

I. V. Vereshchaka,[1] W. Pilewska,[2] M. Zasada,[2] and A. I. Kostyukov[3]

Received June 8, 2018.

In this theoretical study, two-joint equilibrium muscle contractions were simulated to determine the end-point forces created by the hand of the human right upper limb within the horizontal plane. For invariable frontally directed end-point forces, 3D surfaces simulating joint torques (JTs) at the shoulder and elbow joints are reconstructed by defining the characteristic angles (CAs) between the frontal axis and lines from the joint axes to the end-point. The 3D shoulder JTs are presented by planes oriented perpendicularly to the sagittal plane with a downward sagittal skewness; the elbow JT surfaces are essentially nonlinear, showing higher gradients within the left half of the working space. Oppositely directed end-point forces demonstrate the invariance of the JT surfaces that turn about the zero-torque plane while keeping their shapes. Differences between the JTs in the same curvilinear trajectories of the movements (concentric circles) are also analyzed; generation of unvaried (frontally directed) and changed (tangential) end-point forces are compared. Despite the fact that a symmetric pattern in the shoulder JTs is maintained, a transition from the frontal to tangential forces essentially influences the asymmetric pattern of the elbow JTs. The obtained results are discussed with regard to the control of multijoint movements of the limbs in humans.

Keywords: motor control, two-joint movements, upper limb, joint torques, muscle synergy, central commands.

INTRODUCTION

Interrelations between the spatial/time parameters of the movements, forces developed by the muscles in the course of such movements, and motor commands coming to these muscles form a crucial set of problems in the studies of mechanisms controlling limb movements. Application of theoretical and simulation approaches for resolving such problems is undoubtedly expedient.

In a significant part of the movement control studies, relatively fast movements are subjected to the analysis. Methods of kinematics and dynamics are mostly applied in this case. As an example of such an approach, the method proposed by Hollerbach [1], allowing the researcher to consider multijoint movements using internal models of the intersegmental dynamics, should be mentioned. The so-called inverse internal model is usually applied to consider the relations between mechanisms transforming the analyzed movements and central programs addressed to the muscles in these movements [2–4]. Control signals in such models are based on information on the muscle torques defined by inverse dynamics equations. At least partly, the inverse dynamics is formulated through second-order differential equations defining velocities and accelerations for different upper limb segments. An alternative method based on the theories of position-dependent control [5–7] could be suitable for the analysis of rather slow movements or steady states (e.g., under conditions of isometric muscle contractions), when purely equilibrium states of the system of motor control can be applied for the interpretation of interaction of the body with the environment. As an example of such approach

[1] Department of Physical Education, Gdansk University of Physical Education and Sport, Gdansk, Poland.
[2] Faculty of Physical Education, Health, and Tourism, Institute of Physical Culture, Kazimierz Wielki University, Bydgoszcz, Poland.
[3] Department of Movement Physiology, Bogomolets Institute of Physiology, National Academy of Sciences of Ukraine, Kyiv, Ukraine.
Correspondence should be addressed to A. I. Kostyukov (e-mail: kostyuko@biph.kiev.ua).

is the equilibrium point hypothesis proposed by Feldman (for review, see [7, 8]). One of the advantages of the static models is the possibility of taking into consideration nonlinear properties of the neuromuscular system, in particular that of muscle hysteresis [9]. It is much more difficult to incorporate nonlinear elements into models of rapid movements; this is mainly restricted by the necessity of using linear differential equations. Errors in the modeling might be strongly influenced by both incorrect identification of the mechanical parameters (inertia and geometry of the limb segments) and underestimation of nonlinear components in the muscle dynamics.

Recording of slow movements of the upper or lower limb with parallel recording and analysis of EMGs of the involved muscles is ordinarily used to estimate the relationships between the movement *per se* and central commands providing its performance. Such an approach becomes especially effective when the test movements can be repeated many times and, later on, averaged. Recently, slow circular movements of the hand with a fixed wrist have been studied during the action of elastic loads acting tangentially with respect to the movement trajectory [10]. Such an experimental model allowed us to define the torques acting around the shoulder and elbow joints (*joint torques*, JTs), the respective calculations were based on values of the load and lengths of the arm segments. The above study demonstrated the existence of a strict correspondence between the shoulder and elbow JTs and intensities of EMGs recorded from the appropriate muscles. During a complete movement period, each of the torques includes two components, positive and negative, which correspond to the activities of the extensor muscles, respectively. Timings and relative durations of both torque and EMG waves for different joints are dissimilar. In addition to analytical computation of the torque waves [10], a geometrical method was proposed to define exact positions of the points, where JTs change their signs [11]. To distinguish various combinations of activity in the flexors and extensors acting upon different joints, traces of the movements within phases of the latter performed with coinciding (flexor-flexor, extensor-extensor) and opposing (flexor-extensor, extensor-flexor) synergies of the muscles operating different joints were proposed to be analyzed separately [10–13]. A similar procedure for estimation of the interrelationships between JTs and EMGs has been extrapolated on nearly isometric muscle contractions [14, 15], when a tested subject should slowly change the direction of the end-point force. For circular turnings of the force vector, changes in the shoulder and elbow JTs demonstrated sinusoidal patterns and equal durations of the positive and negative components.

The experimental models with visually controlled two-joint movements showed that, at least for sufficiently slow movements, our knowledge of the system statics might be important for the analysis and/or prediction of the commands coming to the muscles from the CNS. In our preceding paper [13], theoretical reconstruction of the JT patterns has been proposed for arbitrary end-point forces with the related analysis of JTs during consecutive changes in the joint angles. The model we have used assumes that the velocities of changes in the central commands to the muscles operating different joints coincide with each other for slow isolated movements at the proximal (shoulder) joint; therefore, the respective commands can be considered *isotropic*. On the contrary, such velocities showed twofold differences for isolated movements at the distal (elbow) joint; this might indicate an *anisotropic* character of the commands to the muscles belonging to different joints. In this our communication, we continue the analysis of the equilibrium states of JTs using Cartesian presentation of the latter, for which the end-point positions in the working space are tested along parafrontal and parasagittal traces. This approach allowed us to present JTs in a 3D form, which makes comparison of the JTs related to different end-point forces more representative.

In conclusion, we would like to point out that the analysis of torque patterns in the multijoint limb movements may include as a basic element the torque modeling for the two-joint systems. Our knowledge of the torques can significantly simplify and expand the neurophysiological analysis of movements in humans using more traditional EMG methods. It may be particularly useful to combine information on the patterns of the torques and EMGs for describing and predicting the synergistic interaction of various muscles in real human movements.

Computer Simulations. Computations and graphical plotting in this study were performed using Origin 8.5 software (OriginLab Corporation, USA). The respective formulas were computed using an internal software language based on operations with the worksheet columns; dimensions

of the worksheets used were 1000 rows (standard) and from 6 to 15 columns. Changes in the fixed parameters in the formulas were provided by replication of basic worksheets.

RESULTS

Description of the Model. The equation shown below was obtained in our previous study [13] in the course of simulation of the equilibrium states of two-joint movements for the case where lengths of the upper and lower arm segments are equal to each other:

$$M_s = Fh_s \sin(\theta - \gamma_s);\ M_e = FL \sin(\theta - \gamma_e). \quad (1)$$

Equation (1) includes apparent expressions for the torques acting around the shoulder and elbow joints. Those combined actions evoke generation of an isometric force $\boldsymbol{F}(\theta)$ at a given end-point of the working space. For a given force magnitude $|\boldsymbol{F}|$ and arm geometry ($L_s = L_e = L$), the end-point force $\boldsymbol{F}(\theta)$ is completely defined by the *characteristic angles* (CAs) γ_s and γ_e; the length parameter h_s is equal to the distance from the shoulder joint axis to the end-point H (Fig. 1A). In accordance with Fig. 1A, the distance between the shoulder axis and the hand is defined as follows:

$$h_s = L[\cos(\gamma_s - \alpha_s) + \cos(\gamma_e - \gamma_s)]; \quad (2)$$

where the γ_e and γ_s CAs are defined depending on the joint angles a_e and a_s:

$$\gamma_s = \tan^{-1}\left[\frac{\sin\alpha_s + \sin(\alpha_s + \alpha_e)}{\cos\alpha_s + \cos(\alpha_s + \alpha_e)}\right]; \gamma_e = \alpha_s + \alpha_e. \quad (3)$$

In accordance with Fig. 1A, the coordinates of the end-point *H*, which are presented implicitly in Eq. (1), may be determined by the following expression:

$$H_x = h_s \cos\gamma_s; H_y = h_s \sin\gamma_s. \quad (4)$$

Changes in the CAs along Parafrontal and Parasagittal Lines. Table 2 presents the sequence of procedures defining the CAs γ_s and γ_e for various hand positions along the parafrontal and parasagittal lines; a schematic representation with exact positioning of the lines and results of simulation is shown in Fig. 2. Pairs of the CAs, γ_s and γ_e, which have been defined along the parafrontal and parasagittal lines, correspond completely to each other. This fact demonstrates an exact coincidence of the knot points and opens a possibility to merge two sets of the curves into 3D surfaces (Fig. 3). It should be noted that projections of the surfaces onto the basic orthogonal planes completely coincide with the initial 2D curves. A symmetric character of the γ_s surface (Fig. 3A) corresponds to both parafrontal and parasagittal sections (Fig. 2A, B, row 2). Parafrontal γ_s sections show the rotational

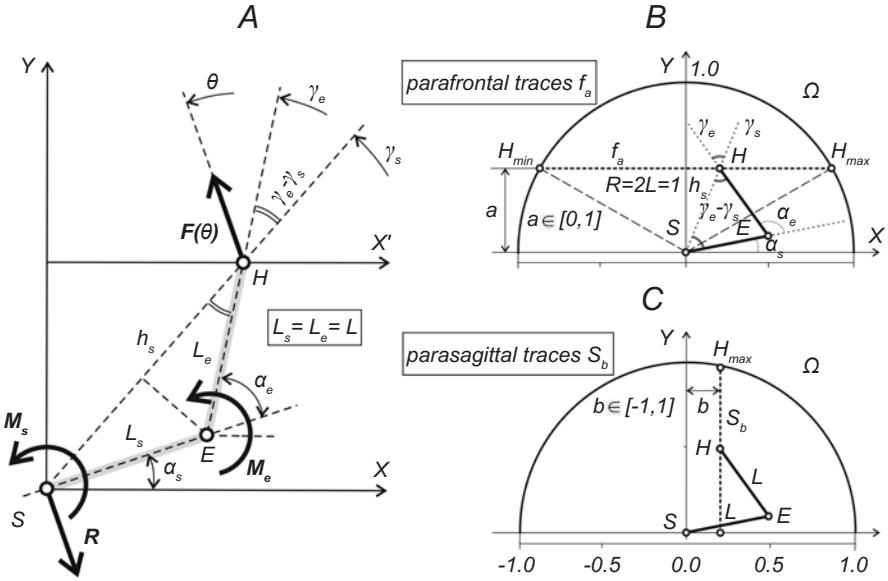

Fig. 1. Definition of the basic geometric parameters of the model (A) and schematic presentation of the parafrontal (B) and parasagittal (C) sections.

symmetry about point $\gamma_s(0) = \pi/2$, satisfying the following conditions:

$$\gamma_s(-x) = \pi - \gamma_s(x). \quad (5)$$

In contrast, the γ_e surface (Fig. 3B) and related sections in Fig. 2 show no symmetry. At the same time, it seems interesting that a strong sagittal symmetry has appeared in the difference of the CAs ($\gamma_e - \gamma_s$), as can be seen in the bottom row of Fig. 2 panels. The symmetry is displayed with respect to a parasagittal plane passing via the shoulder joint.

In general, 3D surfaces $\gamma_s(X)$ and $\gamma_e(X)$ will not depend on the type of initial 2D sections, with no dependence on the type of the traces, orthogonal or curvilinear [13]. Possible variations are explained by different boundaries of the working space accepted in these tests, as well as by differences between steps of changes in the argument.

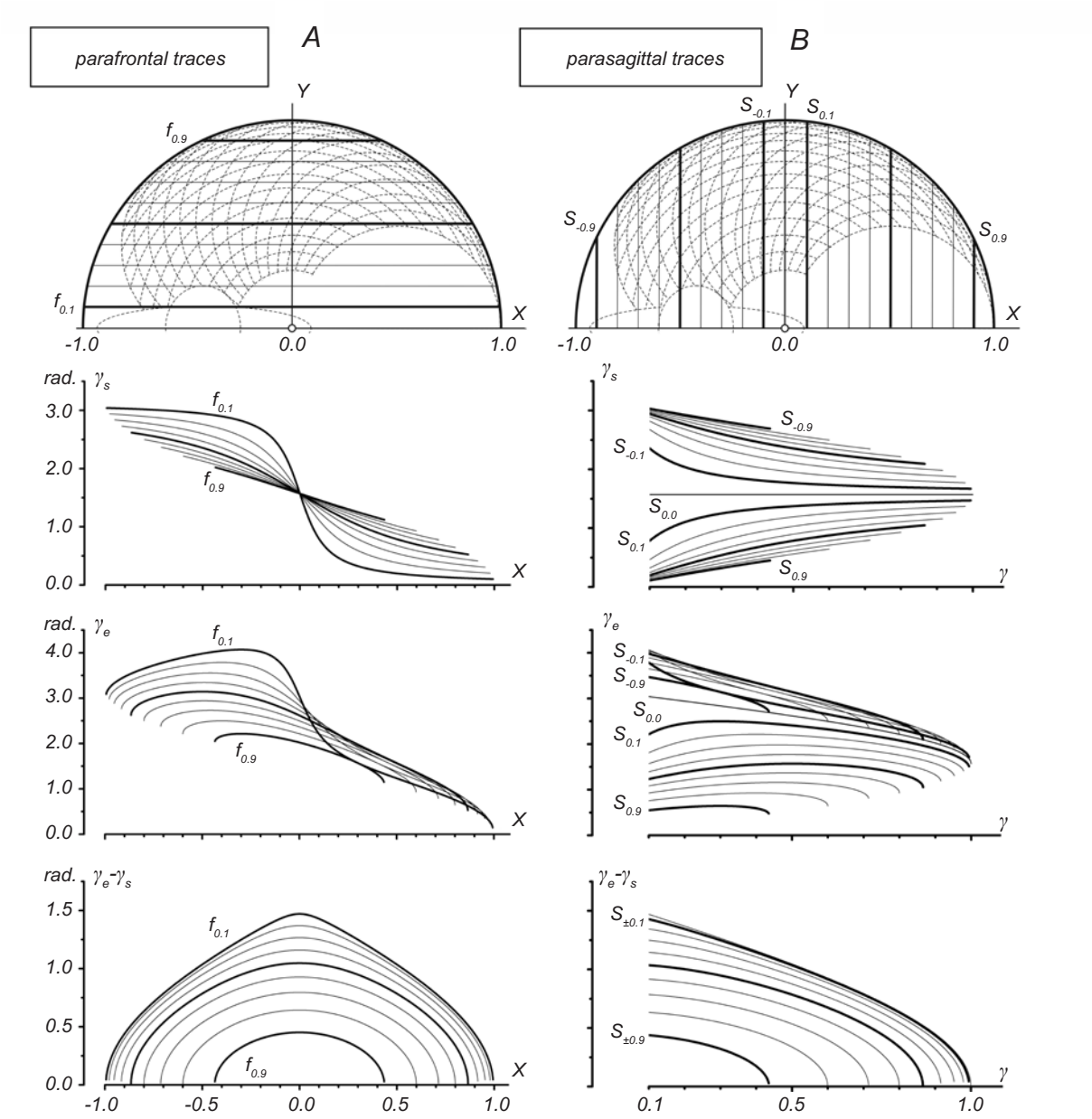

F i g. 2. Changes of the characteristic angles (CAs) γ_s and γ_e and their differences (γ_e -γ_s) in various hand positions within the working space. The positions are changed along the parafrontal (A) and parasagittal (B) traces shown in the upper panels; the lines (f_a, s_b) pass through an interval consisting of 0.1 of the radius of the working space (R = 1). Some of the traces, as well as the corresponding angle curves, are marked by the line thickness for better distinguishing. Dashed lines in the upper panels can help one to create an impression about more realistic boundaries of the real movements; note that some parts of the traces (therefore, the related segments of the curves on the plots) are located outward with respect to the movement boundaries.

T a b l e 1. Sequences of the Procedures Used to Determine the CAs γ_e and γ_s in Various Hand Positions within the Working Space.

	Parafrontal traces *y is fixed; y=a;(a=0.1....0.9);* *x is varied;* $x \in \left[-\sqrt{1-a^2}\,;\sqrt{1-a^2}\right]$;	Parasagittal traces *x is fixed; x=b;(b= –0.9....0.9);* *y is varied;* $y \in \left[0;\sqrt{1-b^2}\right]$;
1	$h_s = \sqrt{x^2+a^2}$;	$h_s = \sqrt{y^2+b^2}$
2	$cos\left(\gamma_e - \gamma_s\right) = \frac{h_s}{2L} = \sqrt{x^2+a^2}$	$cos\left(\gamma_e - \gamma_s\right) = \frac{h_s}{2L} = \sqrt{y^2+b^2}$
3	$\gamma_e - \gamma_s = cos^{-1}\left(\sqrt{x^2+a^2}\right)$	$\gamma_e - \gamma_s = cos^{-1}\left(\sqrt{y^2+b^2}\right)$;
4	$\gamma_s = cos^{-1}\left(\frac{x}{h_s}\right)$;	$\gamma_s = sin^{-1}\left(\frac{y}{h_s}\right)$;
5	$\gamma_e = \gamma_s + \left(\gamma_e - \gamma_s\right)$	$\gamma_e = \gamma_s + \left(\gamma_e - \gamma_s\right)$.

Footnote: Left and right parts are related to changes in the hand position along the parafrontal and parasagittal lines, as shown in Fig. 2A, B (upper row)

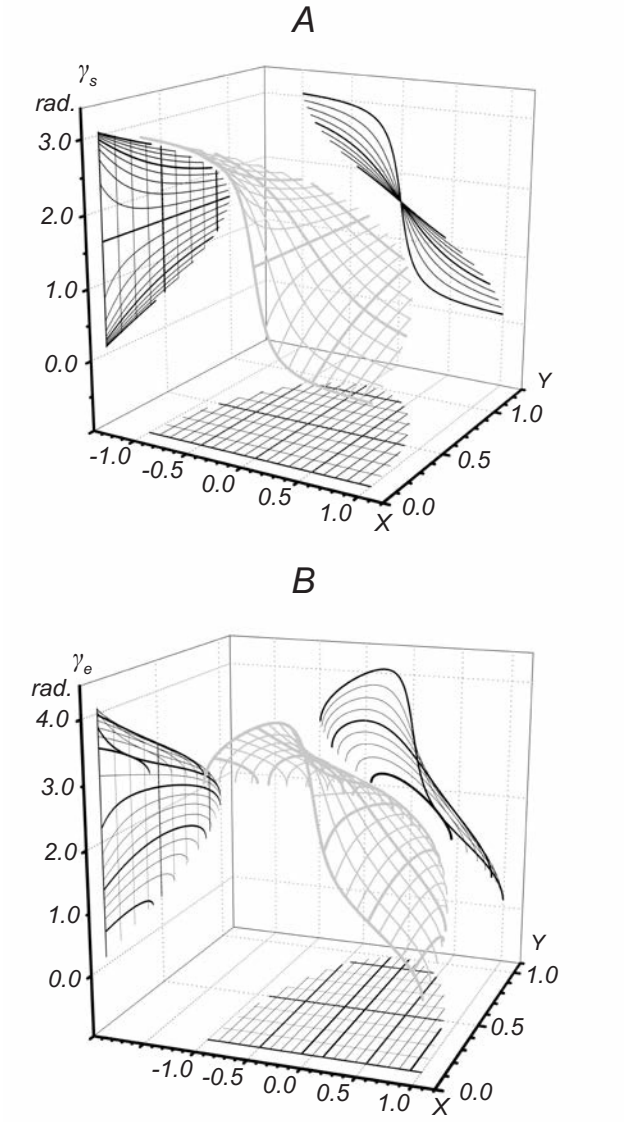

F i g. 3. 3D reconstructions of the CAs γ_s and γ_e based on the sets of their parafrontal and parasagittal traces shown in Fig. 2.

Analysis of the JTs Creating the End-Point Forces in the Frontal Direction. Figure 4 illustrates the JTs that should be created to produce the end-point forces directed in a parallel manner with respect to the frontal plane, i.e., when $\theta = 0$ in Eq. (1). The torques are defined separately for the parafrontal (*A-C*) and parasagittal (*E-F*) traces in accordance with the procedures described in Table 1 and Eq. (1). The shoulder JT is characterized by linear parafrontal and parasagittal traces (Fig. 4A, D); thus, the JT has a planewise shape. The plane is inclining in the sagittal direction, and the JT gets negative values within the entire working space. In contrast, orthogonal traces at the elbow JT demonstrate much more complicated nonlinear shapes; the torques are predominantly negative, being positive within restricted areas at the left part of the working space (compare M_e traces $f_{0.1} - f_{0.4}$ and $s_{-0.1} - s_{-0.9}$ in Fig. 4B, E). Using the parafrontal and parasagittal traces (Fig. 4B, E), it is possible to build a 3D surface for the elbow JT (Fig. 5); considering the simplicity of the shape of the shoulder JT, its 3D reconstruction has not been shown.

The JTs simulate the necessary force reactions of the body, which are directed toward creation of a given end-point force in any point of the working space. The torque 3D surfaces are smooth; they can have linear or nonlinear shapes, which are defined by their dependence on the JTs (on the CAs entering Eq. (1)). When it is necessary to generate the end-point forces, which are invariable within the entire working space, shapes of the torque surfaces will be crucially dependent on the force direction defined by angle θ, while changes in the force magnitude

would only shift them in the vertical direction. For isometric muscle contractions or sufficiently slow movements, a tight relation between the EMGs magnitudes and corresponding JTs does exist [10, 14, 15]. Therefore, it might be assumed that, upon some kind of "activation" of 3D surfaces resembling each other in their shape, definite parts of the torque surfaces also do exist. Such "activation surfaces" are actually related only to the equilibrium states in the system. One can propose the following description of the steady states and transition between these states within the working space. If an initial end-point possesses coordinates (x, y), and the unit vector $\vec{r}$ defines the direction toward the nearest targeted point of the movement, then activation inflows to the muscles can be defined as follows:

$$E_s(x,y,\vec{r}) = E_s^{(1)}(x,y) + E_s^{(2)}(x,y,\vec{r}) = \\ = a_s M_s(x,y) + b_s\left(\frac{\partial M_s}{\partial x} r_x + \frac{\partial M_s}{\partial y} r_y\right); \quad (6)$$

$$E_e(x,y,\vec{r}) = E_e^{(1)}(x,y) + E_e^{(2)}(x,y,\vec{r}) = \\ = a_e M_e(x,y) + b_e\left(\frac{\partial M_e}{\partial x} r_x + \frac{\partial M_e}{\partial y} r_y\right), \quad (7)$$

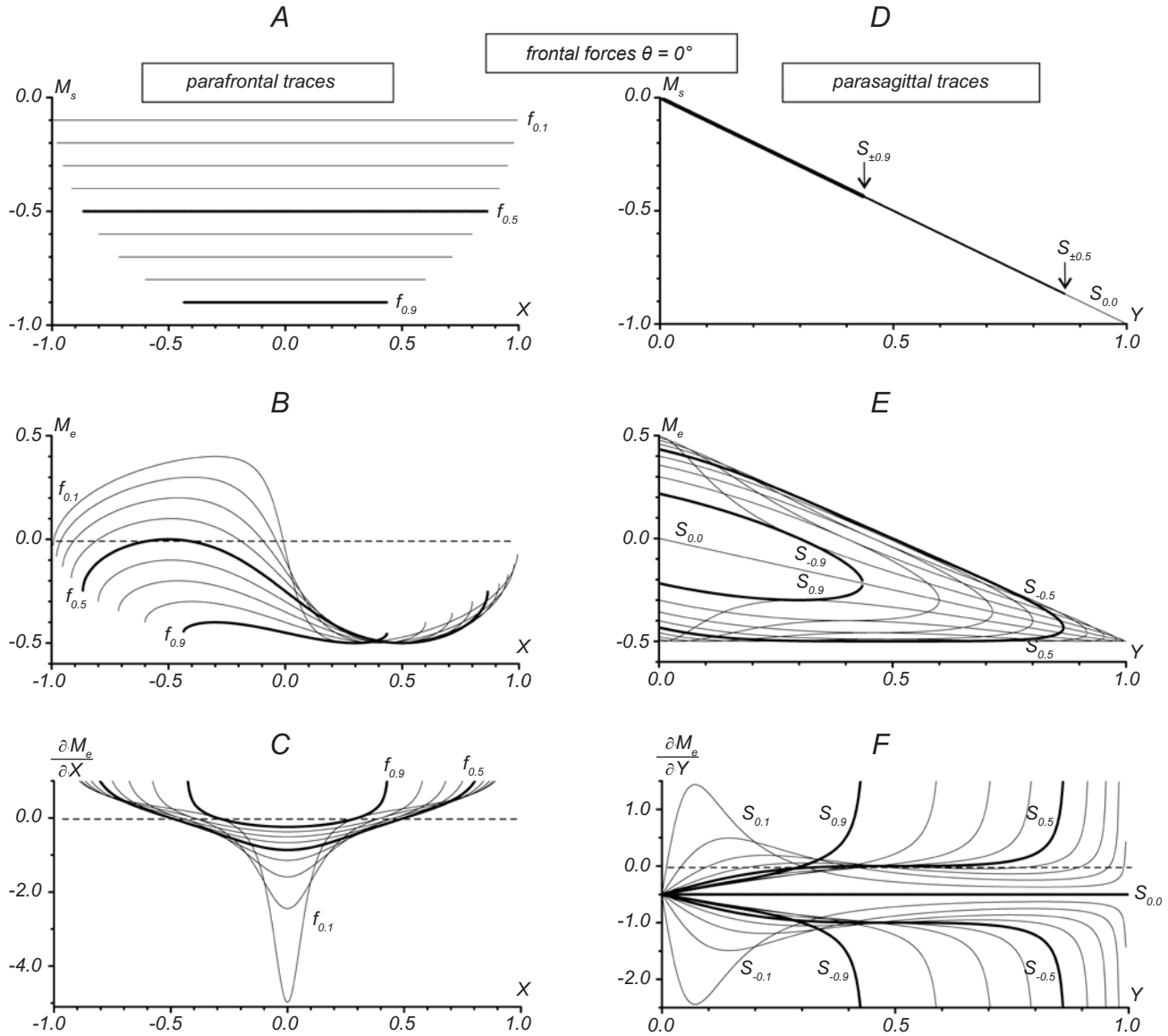

F i g. 4. Computation of the shoulder and elbow JTs (M_s and M_e, respectively) related to generation of the steady end-point forces in the frontal direction ($\theta = 0$); the torques are defined for the parafrontal (A, C) and parasagittal (B, D) end-point transitions. Panels E and F show results of numerical differentiation of the $M_e(X)$ and $M_e(Y)$ dependences. Calibration of the torques is given in arbitrary units defining the action of the unit force applied normally to the lever of the unit length.

where a_s and b_s are the coefficients of transformation of the torque-activation level.

The components $E_s^{(1)}$ and $E_e^{(1)}$ in Eqs.(6, 7) correspond to initial points at the torque surfaces; the components $E_s^{(2)}$ and $E_e^{(2)}$ define changes in the torques at the assumed direction of the movement. Positive/negative values of the torque correspond to predominant activation of the flexor/extensor muscles; coactivation of the antagonists has not been taken into account in this case.

An example of the hypothesized "activation surfaces" returns us to a consideration of the above case of the frontal end-point forces (Figs. 4 and 5). The negativity of M_s signifies that only the shoulder extensors are involved in any movement within the working space. For the parafrontal movement traces, $\frac{\partial M_s}{\partial x} = 0,\ r_x = 1, r_y = 0, \text{and } E_s^{(2)} = 0$; the activity of the extensors is not` changed: $E_s = E_s(1)$. In contrast, any movement in the sagittal direction would be defined by a linear increase in the negativity of M_s: $\frac{\partial M_s}{\partial y} = -1, r_x = 0,\ r_y = 1, \text{and } E_s^{(2)} = -b_s$. As far as the M_e surface is curvilinear, its derivatives $\frac{\partial M_e}{\partial x}$ and $\frac{\partial M_e}{\partial y}$ should be determined in accordance with the shape of the surface. In a general case, the derivatives in Eq. (7) obtain predominantly nonzero values, except for local extrema at both M_e(X) and M_e(Y) traces.

All parafrontal sections of the M_e surface are characterized by the rotational symmetry with respect to the points where the traces cross the parasagittal plane passing via the shoulder joint. This leads to the symmetry of the derivatives $\frac{\partial M_e}{\partial x}$ with respect to the same plane (Fig. 4E). Faster changes in the parafrontal M_e traces in proximity to the zero X coordinate may be one of the reasons for a significant rise in the amplitude of component $E_e^{(2)}$ in Eq. (7). Differences in the slopes of the left and right parts of the M_e surface during parasagittal movements (Fig. 4D, F) may lead to a conclusion that any movement at the right part of the surface will require lesser gradients of the central commands addressed to the muscles. The pattern of the derivative traces ($s_{0.1} - s_{0.9}$ in Fig. 4F) shows that gradients of the M_e torques are smaller at the right part of the working space. Therefore, component $E_e^{(2)}$ in Eq. (7) will be smaller for the movement trajectories within the right part of the working space.

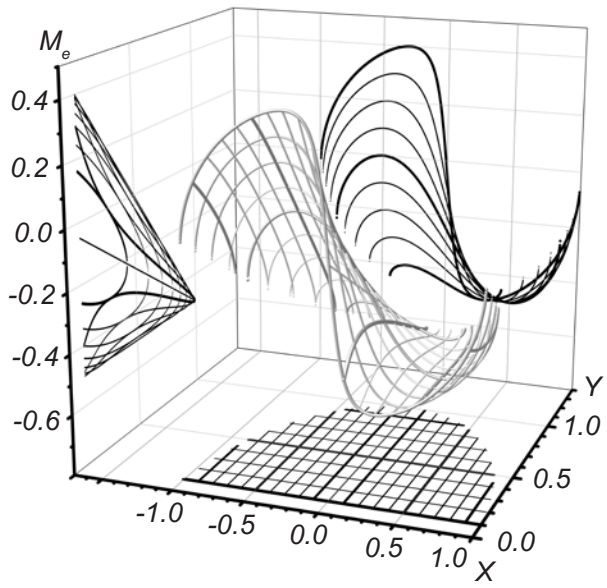

F i g. 5. 3D reconstruction of the elbow torques based on their parafrontal and parasagittal traces shown in Fig. 4C, D.

From the functional aspect, a more expressed steadiness of M_e within the right half of the working space may lead to relative simplicity of the central programs for the movements produced at the right from the shoulder joint, i.e., within a preferred zone of movements for the right upper limb. For the left limb, a similar simplicity in the central programs will be present within the left part of its working space. The above consideration relates, however, only to the elbow joint; due to the symmetry of the M_s plane, such a side-dependent difference is not typical of the shoulder joint.

Comparison of the JTs for Oppositely Directed End-Point Forces. The same trajectories of real movements can be performed under the action of essentially dissimilar external forces requiring the generation of corresponding end-point forces; therefore, the equilibrium JTs, as well as the related motor commands, will also be dissimilar in these cases. Figure 6 describes changes in the equilibrium JTs for the parafrontal movement traces when the end-point force changes its direction to the opposite one; four mutually perpendicular directions of the forces were compared. For the forces directed frontally (Fig. 6A), reversion of the zero-force direction results in change in signs of both shoulder and elbow torques in each point of the working space. Patterns of the parafrontal traces $M_s(X)$ and $M_e(X)$ do not change in this case, and both torque surfaces turn around the zero-torque plane. Similar

turnings of the torque surfaces appear for other pairs of oppositely directed forces (Fig. 6B, C, D). It can be concluded that, for movements performed with the creation of constant end-point forces, the equilibrium torque surfaces are specifically dependent on the force direction; for opposite force directions, the turning symmetry is shown with respect to the zero-torque plane.

The JTs at Circular Movement Traces. Together with parts of the linear traces described above, circular trajectories (or their parts) may also be of interest for simulation of the real movement trajectories. Figure 7 illustrates a comparison of the tangential and frontal end-point forces for a family of the concentric circles; a scheme of estimation of the JTs in the case of tangential forces is shown in Fig. 7A. Coordinates of the moving point at the circular trace with the radius ρ and center $O(x_0, y_0)$ are defined as follows:

$$x = x_0 + \rho\cos\varphi; y = y_0 + \rho\sin\varphi. \quad (8)$$

For a counterclockwise circular movement, the φ angle changes toward the positive direction; the external force F_e and the force created by the hand F are directed along the tangent to a circle at the end-point H. The slope of the force to the abscissa is determined by angle θ, which is connected with angle φ by the expression $\theta = \varphi \pm \pi/2$.

The CAs and torques can be defined in accordance with the earlier-described procedures. By introducing an auxiliary value $\mu = x/y$, it is possible to determine CAs in the following sequence of computation:

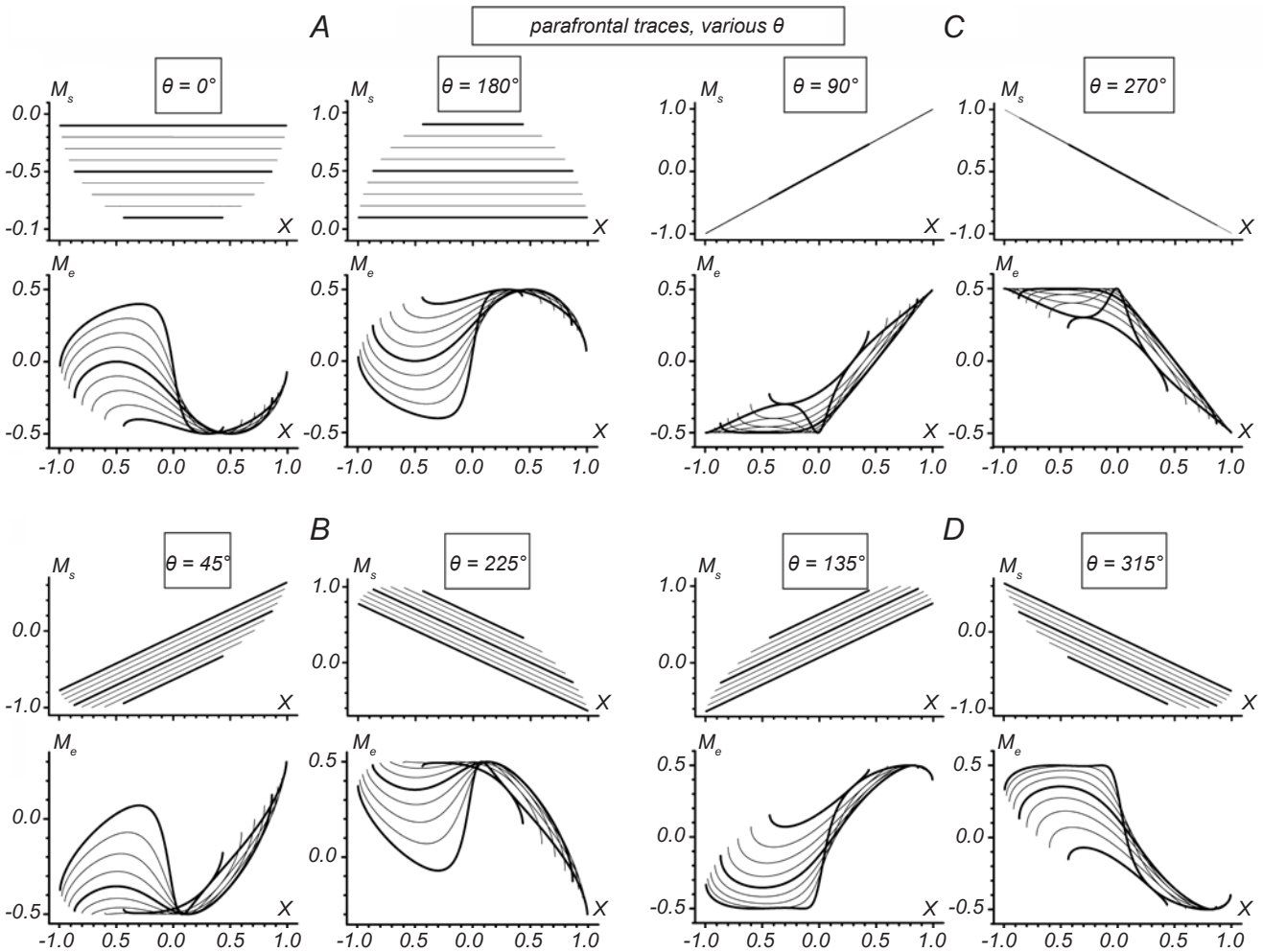

F i g. 6. Comparison of the JTs for four pairs of the end-point forces that are opposite to each other during the same transitions along the parafrontal traces (A–D). The following pairs of the forces are compared: 0, 180° (A); 45, 225° (B); 90, 270° (C), and 135, 315° (D); the torques are calibrated in arbitrary units (as explained in the legend to Fig. 4).

$$h_s = \sqrt{x^2 + y^2} = y\sqrt{\mu^2 + 1}\,; \tag{9}$$

$$\gamma_s = \sin^{-1}\left(\frac{y}{h_s}\right) = \sin^{-1}\left(\frac{1}{\sqrt{\mu^2 + 1}}\right); \tag{10}$$

$$\gamma_e - \gamma_s = \cos^{-1}\left(\frac{h_s}{2L}\right) = \cos^{-1}\left(\frac{y\sqrt{\mu^2 + 1}}{2L}\right); \tag{11}$$

$$\gamma_e = \sin^{-1}\left(\frac{1}{\sqrt{\mu^2 + 1}}\right) + \cos^{-1}\left(\frac{y\sqrt{\mu^2 + 1}}{2L}\right). \tag{12}$$

Experiments corresponding to the scheme in Fig. 7A were described in a paper of our group published earlier [10]. A high degree of correspondence between the averaged EMGs and JTs was observed in these experiments; positive waves of the JTs correlated well with activity of the flexors, whereas negative ones corresponded to EMG waves generated by extensors. Figure 7D shows the simulated torques M_s and M_e for the case of tangential end-point forces applied along the circular paths shown in Fig. 7B. Now, we consider a movement in the counterclockwise direction. This movement is begun at $\varphi = 0$ (axis OO_y). The

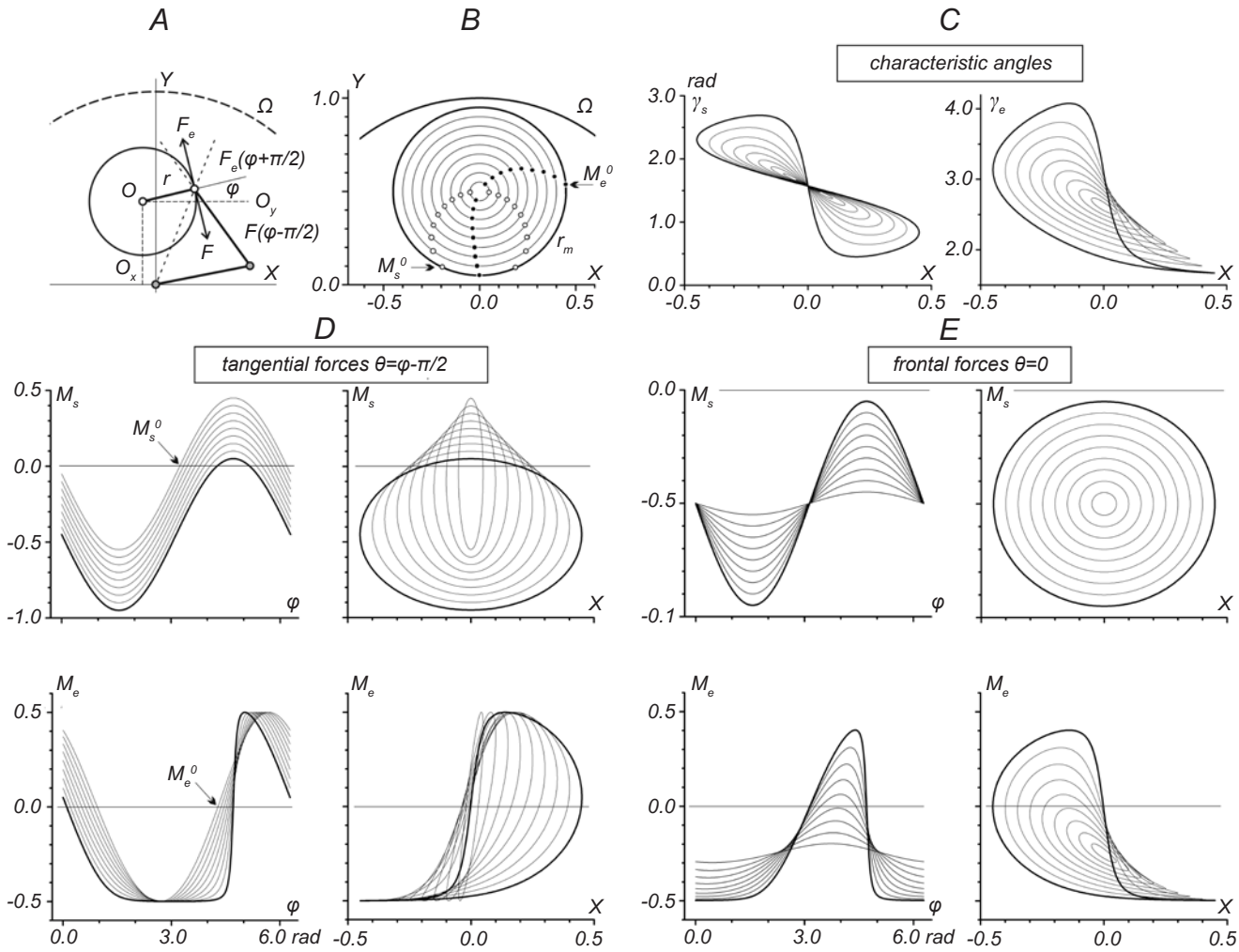

F i g. 7. Comparative analysis of the JTs generating the tangential and frontal forces along the circular traces. A) Scheme explaining generation of the tangential forces at the circular traces; designations O and r are the center and radius of the traces, respectively; φ is the turning angle; $\varphi - \pi/2$ and $\varphi + \pi/2$ are the slope angles of the end-point force (F) and external force (F_e), respectively. The movement traces include nine concentric circles with the center $X = 0$; $Y = 0.5$, and radii $r = 0.05 \ldots 0.45$ (step 0.05). B) The torque traces compared for the tangential (D) and frontal (E) end-point forces depending on the turning angle φ (left columns in D and E) and on the projection of the end-point position on the X axis (right columns in the above panels). Points of the sign reversion at the torque traces (M_s^0 and M_e^0) are shown by open and closed symbols in B. The same ordinate calibration (in arbitrary units) is related for the pairs of $M_{s,e}(\varphi)$ and $M_{s,e}(X)$ plots.

equilibrium state is defined by equation $\boldsymbol{F}_e - \boldsymbol{F} = 0$; a slow counterclockwise movement is provided when the $\boldsymbol{F}_e$ is greater than the $\boldsymbol{F}$. At the beginning position, M_s traces are negative, while M_e ones are positive. With increase in the radii of the circles, the start points of both sets of curves are shifted in the negative direction. Traces $M_s(\varphi)$ comprise identical sinusoids shifting in the positive direction with a decrease in the radii; $M_e(\varphi)$ curves change their shape, keeping the extremal values. Each of the $M_e(\varphi)$ and $M_s(\varphi)$ curves shows the periodicity coinciding with the period of motion.

The points on the movement trajectory, where JTs change their signs, are important for timing of the central commands controlling the movement [10]. These points correspond to the times when antagonistic muscles change their state from "silence" to "activity" and *vice versa*. Such points M_s^0 and M_e^0, which were first determined at the simulated torque curves (Fig. 7D), are superimposed on the motion trajectories (Fig. 7B). These points are located along ellipsoidal curves (described in our earlier simulation study using graphical methods [11]). The vertical axis of the M_s^0 ellipse coincides with the Y axis, which reveals the symmetry of the shoulder JTs with respect to the parasagittal plane passing via the joint. Such a symmetry of the M_s^0 ellipse and the specific asymmetry of the M_e^0 ellipse correspond to the general appearance of the $M_s(X)$ and $M_e(X)$ loops (Fig. 7D, right panels). A decrease in the movement radii makes the $M_s(\varphi)$ loops narrower, shifting them in the positive direction. The asymmetry of $M_e(\varphi)$ loops corresponds of the right-hand protrusion, which decreases gradually with decrease in the movement radii.

For movement traces similar to those described above, Fig. 7E shows the JTs defined when the end-point forces are constant (unchanged) and directed frontally. The torque patterns for such forces differ noticeably from those described above; however, the cyclic elements are still observed in this case. Therefore, the cyclic nature of the torques seems to be provided by the movement recurrence, and a fixed pattern of the end-point forces does not destroy such cyclicity. Despite the same patterns of the CAs in both cases (Fig. 7C), different end-point forces require essentially different torques. Despite keeping a sinusoidal form of the $M_s(\varphi)$ traces for unchanged forces, these traces show a fast amplitude drop with decreases in the radii of the movement traces. At the same time, these traces for tangential forces have a fixed amplitude. For the frontal forces, symmetry effects in the $M_s(X)$ traces are even more clearly expressed due to the addition of the parafrontal symmetry (Fig. 7D, E). Interesting changes were also observed with respect to the elbow torques. To create tangential forces at the circular trajectories, the M_e traces should consist of oscillations of equal amplitude ($M_e(\varphi)$ and $M_e(X)$ in Fig. 7D). At the same time, during generation of fixed frontal forces, these traces become asymmetric, and their amplitudes decrease with a drop in the radii of the circles (Fig. 7E). When comparing $M_e(X)$ traces for the tangential and frontal forces, it can be noticed that protrusions of the torque loops are directed oppositely to each other (Fig. 7D, E). It is possible to observe some resemblance between the $\gamma_e(X)$ and $M_e(X)$ loops (Fig. 7C, E); such a resemblance has been noted above for the parafrontal traces and frontal end-point forces (compare $\gamma_e(X)$ in Fig. 2A and $M_e(X)$ in Fig. 4B). Changes in the end-point forces, such as the tangential ones, can influence the JTs more noticeably compared with conditions of the unvaried forces, and the elbow JTs are more significantly subjected to these influences. In any case, one can see that the JTs are highly sensitive to the pattern of end-point forces.

DISCUSSION

This paper describes further analysis of the JTs in two-joint upper limb movements, which was started in our previous study [13]. In the latter study, the equilibrium JTs were analyzed within the curvilinear coordinate system with the joint angles a_e and a_s as independent coordinates; in this our communication, the same simulation is performed in the Cartesian coordinate system. The general pattern of the CAs, which are defined now along parafrontal and parasagittal traces, agrees with our previous data on both symmetrical pattern of the shoulder CAs and side-dependent asymmetry of the elbow CAs (between the left and right halves of the working space). Some apparent differences between the two types of distribution of CAs in different coordinate systems seem to be mostly related to a discrepancy between the used external boundaries of the working spaces in these simulations.

In simulations of the JTs, the end-point forces $\boldsymbol{F}(\theta)$ are directed arbitrarily with possible changes of angle θ within the 0 to 2π range. In a given point

of the working space, the shoulder and elbow JTs are completely defined in a single-valued manner by Eq. (1). For fixed parameters defining the end-point force ($|\boldsymbol{F}|$; θ), both CAs (γ_s and γ_e) and JTs (M_s and M_e) are represented by smooth 3D surfaces covering the working space. As an example, we have considered 3D surfaces for the case of constant end-point forces acting in the frontal direction ($\theta = 0$). Interestingly, if both the shoulder and elbow CAs exhibit nonlinear shapes, the transitions from CAs to JTs in accordance with Eq. (1) lead to linearization of the JT at the shoulder joint, whereas the elbow JT does not lose the nonlinear mode. Therefore, the elbow JT keeps a nonlinear shape; moreover, shapes of the surfaces CA and JT at the elbow joint even resemble each other. The shoulder JT acquires a plane-wise form, what seems to be related to the complex interaction of the constituent nonlinearities. In any case, the simpler linear form of the 3D torque surface at the proximal joint in comparison with a nonlinear torque surface at the distal joint might be consistent with the concept on the existence of a "leading" joint in the multisegmental limb movements [16]. This hypothesis proposes that planning of a complex movement is simplified by choosing one "leading" joint, which provides the dynamic basement for the entire complex movement. In two-joint upper limb movements, the shoulder joint is usually qualified as the "leading" one due to the higher inertia and stronger musculature of the upper limb link [17–19].

For pairs of oppositely directed end-point forces, surfaces of the corresponding JTs keep their shapes, turning about the zero-torque plane (Fig. 6). Our data allow us to conclude that, at least for movements fulfilled with the creation of constant end-point forces, the equilibrium torque surfaces are specifically dependent on the force direction. For opposite force directions, these surfaces show a turning symmetry with respect to the zero-torque plane. Earlier, we have proposed a classification of the force synergies in accordance with functional modality of the muscles operating different joints, which are activated simultaneously [11]. The coinciding synergy corresponds to simultaneous activation of the muscles of the same modality at both joints (flexors-flexors; extensors-extensors); in the case of opposing synergy, muscles of different modality (flexors-extensors; extensors-flexors) are simultaneously activated. Muscle combinations in both types of effects of synergy depend on the direction of the end-point force; a change in the direction naturally results in the exchange between active and non-active ("silent") muscles. Due to the invariance of the JT surfaces, alteration of the force direction does not change the synergy effects considered within the framework of the aforementioned dichotomy.

Real movement trajectories often contain curvilinear segments; the latter can be approximated by circular traces. In this our study, the JTs are defined for the movement paths, including the set of concentric circles of different radii. The same movements are compared for two types of end-point force, tangentially directed forces that change during the movements and frontally directed forces that do not vary within the entire working space. Due to the presence of some common features in the torque traces of the above two types, essential differences are observed as well. The shoulder JTs demonstrate obvious symmetry with respect to the parasagittal plane passing via the joint, while the elbow JTs are essentially asymmetric. It seems to be important that torques at the proximal joint are characterized by symmetry, and the latter does not disappear with changes in both movement pattern (parafrontal, parasagittal, or circular traces) and type of the generated force (unvaried or changing within the working space). On the contrary, torques at the distal joint are highly sensitive to both end-point positioning and type of the end-point forces. With unvaried frontally directed forces, the steepness of the elbow torque surface is significantly higher at the left part of the parasagittal plane passing via the proximal joint. Such an asymmetric pattern of the elbow torques may be kept for various movement traces (compare Figs. 6 and 7). *Vice versa*, a transition from the frontal to the tangential end-point forces evokes strong transformation of the elbow JT traces. In the former case, a higher steepness of the traces is typical of the left half of the working space; in the latter case, this order is reversed (bottom row in Fig. 7). Therefore, the pattern of end-point forces crucially influences the JTs.

We considered static conditions for the two-joint system only for the cases of non-zero end-point forces. When the mentioned forces are small or absent, the system may formally be in an uncertain state; therefore, the end-point positions in the working space are not predetermined. The effects of uncertainty can also be inherent to low-intensity efferent inflows to the relaxed muscles. On the other hand, a powerful source of uncertainty effects

can be the interaction of agonist-antagonist pairs of the muscles or muscle groups, when reciprocal changes in the lengths of these muscles during the movement can in some cases modify the expression of hysteresis aftereffects [9, 20–22].

Behavioral studies using postural test tasks have demonstrated that the tested subjects frequently use muscle co-contraction as a strategy for stabilization of the limb joints in the presence of external loadings [23]. Humans are also able to modulate independently the relative balance of co-contraction and limb stiffness in different spatial directions [24] and at different joints [25]. At the same time, co-contraction of the antagonistic muscles should inevitably increase the energy costs of real movements.

Despite the existence of close relationships between the JTs and intensities of EMGs of the respective muscles in real circular movements performed under conditions of application of tangential loads, noticeable EMG activities recorded from the elbow and shoulder muscles may often be expressed in sites that are out of the borders of the correspondent torque waves [10]. This phenomenon might be related to a more complicated arrangement of the joints compared with that in a simple pivotal model used to define the JTs in the above-cited study. It seems that the biomechanics of the elbow and shoulder joints can introduce additional elements of indeterminacy into their torques. A complex geometry of the rotational movements in the shoulder joint was mentioned in the study of Hill et al. [26]; the elbow joint has also been considered an assemblage of three interactive joints [27]. It should be noted that a simplified model of the upper limb muscles as belonging exclusively to the elbow or shoulder joints is certainly oversimplified; sites of the force applications can be considered fixed only for the monoarticular muscles, while a procedure of identification of such sites for the biarticular muscles is much more complex [28].

From the functional aspect, a more expressed steadiness of the elbow JT within the right half of the working space may lead to relative simplicity of the central programs for the movements produced rightward from the shoulder joint (in other words, within a preferred zone of movements of the right upper limb). For the left limb, similar simplicity of programming will be obvious within the left part of the working space. If we consider movements by two upper limbs within a horizontal plane [12], this comment obviously corresponds to our everyday experience; it is much more convenient to move each arm, left or right, within its "own" half of the working space, at the left or right side, respectively. Therefore, at least for the elbow muscles, such a side preference in the case of the frontal and tangential end-point forces might be related to essentially lower slopes of the torque surfaces within these areas of the working space (Figs. 4 and 7). Therefore, any movements within the above areas will require smaller changes in the central commands coming to the muscles. On the other hand, the symmetry effects in the shoulder torque surfaces, as well as their planar shapes for some types of the end-point forces, mean that our results could be consistent with the leading joint hypothesis proposed by Dounskaia [16].

Under conditions of relatively slow movements, the parameters of the end-point force vector, as well as the direction of the intended movement, are crucial for defining necessary changes in the JTs. For a given end-point force, 3D surfaces of the JTs actually "create certain rules" of their change in any direction of the subsequent movement. In other words, one can consider two projections of the real movement trajectory on the shoulder and elbow JT surfaces, respectively; these torque traces predetermine central commands sent to the muscles of corresponding joints. The tight interdependence, which exists between the JTs and corresponding EMGs [10, 12, 14, 15], allows us to assume the existence of some 3D "activation" surfaces that could partly resemble shapes of the JTs surfaces. Such "activation" surfaces actually are related only to the steady (equilibrium) states in the system under study, as follows from the equilibrium point hypothesis [7, 8]. It seems quite obvious that real movements with nonzero velocities would introduce significant changes into central commands controlling these movements; therefore, the analysis of the movements should require application of the dynamic methods [1–4].

CONCLUSIONS

The two-joint equilibrium muscle contractions providing creation of the end-point forces developed by the hand of the human right upper limb at positioning within the horizontal plane have been simulated. The 3D surfaces of distribution of the JTs

are reconstructed for the invariable end-point forces directed frontally. The shoulder JTs form the planes oriented perpendicularly with respect to the sagittal plane, and a downward skewness with respect to the sagittal direction is observed. The 3D surface of the elbow JT is essentially nonlinear, showing more expressed gradients of the torque within the left part of the working space for the right upper limb. For pairs of oppositely directed end-point forces, surfaces of the corresponding JTs keep their shapes when turning about the zero-torque plane.

Acknowledgment. This work was supported by the DS_WF │1│16│2017 – Statutory Research of the Physical Education Department, Gdansk University of Physical Education and Sport, Poland.

This is a theoretical/simulation study. Therefore, the statement on the compliance of the work to the existing international ethical normatives for experimental studies is not necessary.

The authors, I. V. Vereshchaka, W. Pilewska, M. Zasada, and A. I. Kostyukov, declare that the research was conducted in the absence of any commercial or financial relationships that could be construed as a potential conflict of interest; there are no conflicts between co-authors.

REFERENCES

1. J. M. Hollerbach, "Computers, brains, and the control of movement," *Trends Neurosci*., **5**, 189-192 (1982).
2. D. M. Wolpertand and Z. Ghahramani, "Computational principles of movement neuroscience," *Nat. Neurosci*., **3**, 1212-1217 (2000).
3. D. M. Wolpert and M. Kawato, "Multiple paired forward and inverse models for motor control," *Neural Netw*., **11**, 1317-1329 (1998).
4. M. Kawato, "Internal models for motor control and trajectory planning," *Cur. Opin. Neurobiol*., **9**, No. 6, 718-727 (1999).
5. E. Bizzi, N. Hogan, F. A. Mussa-Ivaldi, and S. Giszter, "Does the nervous system use equilibrium-point control to guide single and multiple joint movements?" *Behav. Brain Sci*., **15**, No. 4, 603-613 (1992).
6. A. G. Feldman, "Once more for the equilibrium point hypothesis (λ model)," *J. Mot. Behav*., **18**, 17-54 (1986).
7. A. G. Feldman, "Space and time in the context of equilibrium-point theory," *Wiley Interdiscip. Rev. Cogn. Sci*., **2**, No. 3, 287-304 (2011).
8. A. G. Feldman, "The relationship between postural and movement stability. Progress in motor control," *Adv. Exp. Med. Biol*., **957**, 105-120 (2016).
9. A. I. Kostyukov, "Muscle hysteresis and movement control: a theoretical study," *Neuroscience*, **83**, No. 1, 303-320 (1998).
10. T. Tomiak, T. I. Abramovych, A. V. Gorkovenko, et al., "The movement- and load-dependent differences in the EMG patterns of the human arm muscles during two-joint movements (a preliminary study)," *Front. Physiol*., **7**, No. 218 (2016); doi: 10.3389/fphys.2016.00218.
11. A. I. Kostyukov, "Theoretical analysis of the force and position synergies in two-joint movements," *Neurophysiology*, **48**, No. 4, 287-296 (2016).
12. T. Tomiak, A. V. Gorkovenko, A. N. Tal'nov, et al., "The averaged EMGs recorded from the arm muscles during bimanual "rowing" movements," *Front. Physiol*., **6**, No. 349 (2015); doi: 10.3389/fphys.2015.00349.
13. A. I. Kostyukov and T. Tomiak, "The force generation in a two-joint arm model: analysis of the joint torques in the working space," *Front. Neurorobot*., **12**, No. 77 (2018); doi: 10.3389/fnbot.2018.00077.
14. O. V. Lehedza, A. V. Gorkovenko, I. V. Vereshchaka, et al., "Comparative analysis of electromyographic muscle activity of the human hand during cyclic turns of isometric effort vector of wrist in opposite directions," *Int. J. Physiol. Pathophysiol*., **61**, No. 2, 3-14 (2016).
15. O. V. Lehedza, "Manifestations of hysteresis in EMG activity of muscles of the human upper limb in generation of cyclic isometric efforts," *Neurophysiology*, **49**, No. 3, 220-225 (2017).
16. N. Dounskaia, "The internal model and the leading joint hypothesis: implications for control of multi-joint movements," *Exp. Brain Res*., **166**, No. 1, 1-16 (2005).
17. N. Dounskaia and J. Goble, "The role of vision, speed and attention in overcoming directional biases during arm movements," *Exp. Brain Res*., **209,** No. 2, 299-309 (2011).
18. N. Dounskaia, J. Goble, and W. Wang, "The role of intrinsic factors in control of arm movement direction: implications from directional preferences," *J. Neurophysiol*., **105**, No. 3, 999-1010 (2011).
19. N. Dounskaia and W. Wang, "A preferred pattern of joint coordination during arm movements with redundant degrees of freedom," *J. Neurophysiol*., **112**, No. 5, 1040-1053 (2014).
20. A. I. Kostyukov, "Muscle dynamics: dependence of muscle length on changes in external load," *Biol. Cybern.*, **56**, Nos. 5/6, 375-387 (1987).
21. A. I. Kostyukov and O. E. Korchak, "Length changes of the cat soleus muscle under frequency-modulated distributed stimulation of efferents in isotony," *Neuroscience*, **82**, No. 3, 943-955 (1997).
22. A. V. Gorkovenko, S. Sawczyn, N. V. Bulgakova, et al., "Muscle agonist-antagonist interactions in an experimental joint model," *Exp. Brain Res*., **222**, 399-414 (2012).
23. T. E. Milner and C. Cloutier, "Damping of the wrist joint during voluntary movement," *Exp. Brain Res*., **122**, No. 3, 309-317 (1998).
24. E. Burde, R. Osu, D. W. Franklin, et al., "The central nervous system stabilizes unstable dynamics by learning optimal impedance," *Nature*, **414**, No. 6862, 446-449 (2001).

25. P. L. Gribble and D. J. Ostry, "Independent coactivation of shoulder and elbow muscles," *Exp. Brain Res*., **123**, No. 3, 335-360 (1998).
26. A. M. Hill, A. M. J. Bull, A. L. Wallace, and G. R. Johnson, "Qualitative and quantitative descriptions of glenohumeral motion," *Gait Posture*, **27**, No. 2, 177-188 (2008).
27. C. D. Bryce and A. D. Armstrong, "Anatomy and biomechanics of the elbow," *Orthop. Clin. North Am*., **39**, No. 2, 141-154 (2008).
28. B. M. Van Bolhuis, C. C. Gielen, and G. J. van Ingen Schenau, "Activation patterns of mono- and bi-articular arm muscles as a function of force and movement direction of the wrist in humans," *J. Physiol.,* **508**, Part 1, 313-324 (1998).